



ELSEVIER

Available online at www.sciencedirect.com

SCIENCE @ DIRECT®

Physica A III (III) III-III

PHYSICA A

www.elsevier.com/locate/physa

Injection locking near a stochastic bifurcation: the dc SQUID as a case study

A.R. Bulsara^{a,*}, J.A. Acebrón^b, W.-J. Rappel^b, A. Hibbs^c,
L. Kunstmanas^c, M. Krupka^c

^a*Space and Naval Warfare Systems Center, Code 2363, 49590 Lassing Road,
San Diego, CA 92152-6147, USA*

^b*Physics Dept., Univ. of California San Diego, La Jolla, CA 92093, USA*

^c*Quantum Applied Science and Research, 6730 Mesa Ridge Rd. Ste A, San Diego, CA 92121, USA*

Received 15 October 2002

Abstract

We examine the response of a 2D nonlinear oscillator (exemplified in this work by the two-junction superconducting quantum interference device - SQUID) subject to a weak time-periodic target signal, just past the onset of a saddle-node bifurcation. Adjusting the control parameters of the device allows us to identify a regime wherein the response (characterized by an output signal-to-noise ratio at the target frequency) is maximal. The phenomenon has the flavor of the well-studied stochastic resonance effect but is, in fact, shown to arise from a nonlinear *deterministic* resonance in the “running solution” regime. Our results are presented in the context of experimental results.

Published by Elsevier Science B.V.

PACS: 05.40.+j; 02.50.Ey; 85.25.Dq

Keywords: Stochastic bifurcation; Resonance; Signal amplification

1. Introduction

Nonlinear dynamic systems exhibit a broad spectrum of interesting behavior, often mediated by background noise that may be either external or present as a noise-floor in the system/device. Among all these phenomena, the *Stochastic Resonance* (SR) effect has been well studied in the past 2 decades [1–3]. In this effect, an appropriate

* Corresponding author.

E-mail address: bulsara@spawar.navy.mil (A.R. Bulsara).

amount of system noise can lead to an enhancement of the response. The literature is suffused with a plethora of definitions of SR; this ambiguity is mainly because a form of noise-mediated signal amplification occurs in a large class of dynamic and non-dynamic (e.g. threshold) systems, and also for a large class of input signal waveforms and background noise statistics. For systems subject to a time-sinusoidal input signal in a noise-floor (usually taken to be Gaussian), the output SNR measured at the target signal frequency suffices to characterize the response; this has led to the definition of SR as a true resonance, the matching of an external deterministic (signal) frequency with a characteristic internal stochastic frequency (the transition rate between stable steady states in the presence of the noise alone) [4–6]. Many of the experiments done to date, in the physics community, concern this class of systems and inputs.

The early experiments aimed at demonstrating the SR effect in a real system included a series of experiments [7,8] on a two-junction (or dc) SQUID, aimed at exploring further the noise-mediated dynamics of the system. More recent experiments [9,10] yielded behavior that was, at first glance, strikingly similar to SR. However, subsequent considerations showed that this behavior could not, in fact, be the same because the noise had not been manually adjusted during the experiment; the system noise was due mainly to thermal noise in the junctions, together with noise injected into the system from the readout electronics, the net result being a Gaussian noise-floor in the presence of which the “resonance” in the output SNR (measured at the fundamental frequency of the input time-sinusoidal target signal) was realized as a function of two *deterministic* control parameters which could be adjusted *independently* of the input SNR.

Clearly, the experimental observations in the dc SQUID experiment point to a phenomenon that although similar to SR is, probably, a deterministic resonance (even though the output SNR is maximized at this resonance). The (overdamped) dc SQUID is a 2D system; recent theoretical work has provided a very good picture of the dynamics relevant to the phenomena outlined above, and now affords an explanation of the experimental results. In this work, we examine the dc SQUID dynamics in the context of the 1997 experiments [9,10]. First, however, we provide a brief description of the dc SQUID dynamics, together with a description of the 1997 experiments and the results obtained therein.

2. Background: experiments on the driven dc SQUID

The dc SQUID consists of two Josephson junctions inserted into a superconducting loop [11,12]. Conventionally, the voltage measured across the junctions is taken as the SQUID’s “output”; instead, we take the circulating current I_s (experimentally measured via the flux induced in a second, closely coupled, SQUID).

In the presence of an external magnetic flux Φ_e , one obtains [11,12] a loop flux consisting of the (geometrical) component Φ_e together with a contribution arising from the induced circulating or shielding current I_s that tends to screen the applied flux: $\Phi = \Phi_e + LI_s$, L being the loop inductance. The Josephson currents in each arm of the “interferometer” are $I_0 \sin \delta_1$ and $I_0 \sin \delta_2$, with the junctions assumed to be identical with critical currents I_0 , and with $\delta_{1,2}$ being the quantum phases. The wave-function

must remain single-valued around the SQUID loop, leading to the phase continuity condition, $\delta_2 - \delta_1 = 2\pi n - 2\pi\Phi/\Phi_0$, n being an integer, and $\Phi_0 \equiv h/2e$ the flux quantum. Combining the above equations and setting $n = 0$, we compute the (experimentally observable) circulating current I_s in terms of the quantum-mechanical phase angles: $\beta(I_s/I_0) = \delta_1 - \delta_2 - 2\pi(\Phi_e/\Phi_0)$, $\beta \equiv 2\pi LI_0/\Phi_0$ being the nonlinearity parameter. In the absence of noise and the target (time-sinusoidal) magnetic flux, one can obtain [11,12] equations for the currents in the two arms of the SQUID via a lumped circuit representation [11]; expressed via the Josephson relations $\dot{\delta}_i = 2eV_i/\hbar$ linking the voltage and the quantum phase difference across the junction i , these equations take the form:

$$\tau \dot{\delta}_i = \frac{I_b}{2} + (-)^i I_s - I_0 \sin \delta_i, \quad i = 1, 2, \quad (1)$$

where $\tau \equiv \hbar R e / 2$, R being the normal state resistance of the junctions. In the experiments [9,10], the dc bias current (applied symmetrically) and flux are externally controllable. This is a critical point, since, as will become evident below, it permits us to manipulate the shape of the 2D potential function that characterizes the SQUID dynamics and thereby the input–output transfer characteristic (TC) that governs the response. Rescaling the time by τ/I_0 , one can write the above in the form $\dot{\delta}_i = -\partial U/\partial \delta_i$ with the 2D potential function defined as

$$U(\delta_1, \delta_2) = -\cos \delta_1 - \cos \delta_2 - J(\delta_1 + \delta_2) + (2\beta)^{-1}(\delta_1 - \delta_2 - 2\pi\Phi_{ex})^2, \quad (2)$$

in terms of the dimensionless quantities $J \equiv I_b/(2I_0)$ and $\Phi_{ex} \equiv \Phi_e/\Phi_0$.

The junctions are superconducting when the potential (2) has stable minima; in this configuration, after a brief transient, the phase angles $\delta_{1,2}$ achieve constant steady-state values and one obtains the conditions for the extrema via $\dot{\delta}_{1,2} = 0$. For the stable steady states this leads to the current equations

$$I_b = I_0(\sin \delta_1 + \sin \delta_2), \quad 2I_s = I_0(\sin \delta_2 - \sin \delta_1). \quad (3)$$

Using the phase continuity relation, we may obtain [13,14] an expression for the circulating current which defines a multi-valued (hysteretic) transfer characteristic (TC) in the superconducting regime. For $J = 0$ one obtains hysteresis for any nonlinearity β ; for $0 < J \leq 1$, hysteresis occurs over some range of β . For a given β , J controls the hysteresis loop width with conservation (3) intact. When this balance is exceeded, however, a finite voltage V (corresponding to a normal loop current V/R) appears across the device. In this regime, pairs of potential minima and maxima coalesce to yield a critical profile characterized by points of inflexion; the potential consists of a series of flat segments connected by steep “ramps”. Past this point, the slope of the flat segments increases and one obtains oscillatory solutions for the phases δ_i (modulo 2π) and the circulating current I_s . A *saddle-node* bifurcation has occurred [15,16]; the oscillatory solutions have a frequency that depends on the control parameters I_b and Φ_{ex} , and this frequency is zero at the onset of the bifurcation, increasing as a function of the control parameters as one goes deeper into the oscillatory or “running” regime.

One might expect to obtain the best response when the TC is non-hysteretic since, in general, the optimal response occurs in the linear or quasi-linear regime. It seems natural, therefore, to bias the SQUID into the non-hysteretic regime. Before exploring

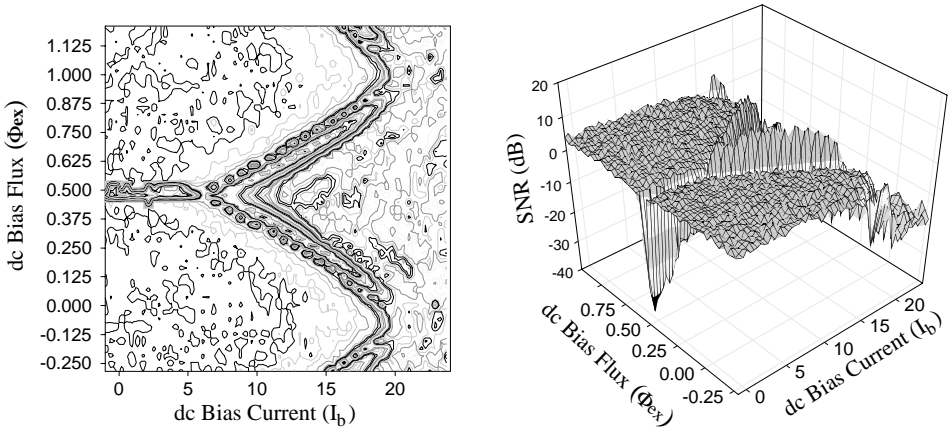


Fig. 1. Contour plot (left) and 3D view of same data (right), showing SNR increase (at target signal frequency 97 Hz) vs. applied bias current I_b (μA) and dc flux Φ_{ex} . $\beta \approx 1.25$. Dark zones correspond to maximum SNR response.

this further, we offer a brief account of the experiments and results that lead to the theoretical work of the past 3 years.

The experimental setup [9,10] comprised two inductively coupled Nb dc SQUIDs in a shielded liquid helium dewar. The measurement (M-) SQUID was operated in the conventional manner and measured the flux state of the switching (S-) SQUID via inductive coupling to the circulating current I_s . The S-SQUID was operated as a free-running nonlinear dynamic device, i.e., not in the (conventional) flux-locked configuration [11]. The variation of I_s as a function of Φ_{ex} produced the input–output TC characterizing the two-SQUID system.

The response of the S-SQUID to a steady sine wave input signal of frequency 97 Hz is shown in Fig. 1. The signal amplitude was of order $100\mu\Phi_0$ (2×10^{-19} Wb). The z-axis in Fig. 1 is the difference between the SNR at the output and the effective SNR applied to input. For low I_b , the SQUID operates in the hysteretic part of the TC with a multistable potential energy function. In this regime, one expects the “conventional” SR effect, or some variation thereof, to dominate the response, as the noise induces activation over the energy barrier. The surfaces in Fig. 1 are periodic in Φ_{ex} (due to the Josephson term in (1)), with $\Phi_{ex} = n/2$ (n odd) corresponding to a symmetric potential. The symmetric potential is also where one obtains the maximal SNR gain (in the fundamental of the response), below the critical point where conservation relations (3) hold. At higher bias currents, the TC becomes non-hysteretic with an accompanying split (at the critical point which defines the onset of the running regime) in the SNR response. For any I_b , the separation of flux values between the SNR peaks corresponds to the separation of the regions of maximum gradient in the TC [9,10,13,14]. The location of the split (as well as the SNR gain) depends on the β value of the SQUID. While the response behavior at low-to-moderate I_b can be well described in the context of conventional SR, the explanation of the response characteristics at and past the SNR

split (in Fig. 1), is not as clearcut. It is tempting to explain this as a conventional SR effect, until one realizes that the SNR gain is obtained in the (I_b, Φ_{ex}) parameter space, with no direct manipulation of the input SNR. Clearly, there is a dynamical effect on the noise-floor for a given set of bias conditions; separately plotting the output signal and noise [9,10] shows that they do change (but do not “track” each other) as the bias conditions are changed. In this configuration, it is also impossible to express the “stochastic resonance” via a matching of deterministic and stochastic time scales (Section 1). These observations are the starting point for our theoretical attempts to explain the behavior shown in Fig. 1 particularly in the oscillatory or running regime, in which we observe a non-hysteretic TC.

3. Stochastic saddle-node bifurcation

Recent calculations [13] can predict the critical point (J_c, Φ_{exc}) at which the saddle node bifurcation to the running regime occurs. The spontaneous oscillation period tends to infinity very close to Φ_{exc} , with the regime of the oscillatory solutions increasing with J (for fixed Φ_{ex}).

Our first task is to compute the frequency of the oscillating solutions, and its scaling behavior in terms of a “distance” from the critical point (obtained by setting the lhs of (1) to zero). This is accomplished [15] via a normal form analysis about the critical point, whereby the dynamics can be separated into a pair of independent ODEs for two variables evolving with well-separated time constants. Dropping the “fast” variables, we are left with a first-order ODE (the normal form that characterizes this bifurcation) for the relevant or “slow” variable; in turn, we can integrate this ODE and obtain the oscillatory solution which yields the period [15]

$$T = \pi/\sqrt{F\alpha}. \quad (4)$$

Here, $F = b(J - J_c)$, the distance from the critical point, and (b, α) have been explicitly evaluated in Ref. [15]. The oscillation period T obeys the characteristic square-root scaling law [16] for this class of bifurcations. While this is not a new observation, we must point out that being able to compute the period (including all prefactors) exactly, constitutes an important first step towards understanding, and possibly exploiting, the nonlinear behavior close to the bifurcation. As expected, expression (4) agrees very well [15] with numerically obtained values as long as we are close to the bifurcation, i.e., the separation $J - J_c$ is small for a given dc bias Φ_{ex} . Increasing β leads to a shrinking of the separation $J - J_c$ over which the normal form accurately portrays the dynamics. It is worth noting [18] that globally coupling SQUIDs postpone the onset of the saddle node bifurcation. The oscillation frequency also decreases as the coupling strength is increased, vanishing for a critical coupling strength.

We now introduce, into the theory, a noise-floor $\zeta(t)$, taken to be Gaussian and delta correlated, having zero mean and variance $2D$: $\langle \zeta(t) \rangle = 0$, $\langle \zeta(t)\zeta(s) \rangle = 2D\delta(t - s)$. Note that, in practice, there may be a variety of noise sources (e.g. the readout electronics) that lead to a noise-floor having a finite correlation time. Then, in general, the normal form dynamics (and therefore the period T) are noise-dependent. In the presence of a

very small noise intensity, however, we may add the noise $\zeta(t)$ phenomenologically to the rhs of the normal form [17]. The resulting “augmented normal form” provides a very good (qualitative at least) description of the noisy dynamics near the bifurcation. Under these conditions, one obtains a distribution of oscillation frequencies with a deterministic mean T^{-1} and a noise-dependent mode [17].

We do not do well any further on the line of reasoning in the preceding paragraph, referring instead to our earlier work [15,17]. Instead, we now return to the original SQUID dynamics (1), augmented by the Johnson noise terms $\zeta_i(t)$, $i=1,2$ where the noise from each junction is assumed to have zero mean and the same intensity $2D$. The noise terms are independent: $\langle \zeta_i(t)\zeta_j(s) \rangle = 2D\delta_{ij}\delta(t-s)$. Then, the coupled equations (1) lead to a Fokker Planck equation (FPE) for the probability density $\rho(\delta_1, \delta_2, t)$ [19]

$$\frac{\partial \rho}{\partial t} = D \left[\frac{\partial^2 \rho}{\partial \delta_1^2} + \frac{\partial^2 \rho}{\partial \delta_2^2} \right] - \frac{\partial}{\partial \delta_1} (v_1 \rho) - \frac{\partial}{\partial \delta_2} (v_2 \rho) \quad (5)$$

and

$$v_i(\delta_1, \delta_2) = J + (-)^i \beta^{-1} (\delta_1 - \delta_2 - 2\pi n - 2\pi \Phi_{ex}) - \sin \delta_i, \quad i = 1, 2, \quad (6)$$

where $v_{1,2}$ are the drift terms (with 2π -periodicity in δ_1 and δ_2), and the density function is normalized, $\int_0^{2\pi} \int_0^{2\pi} \rho(\delta_1, \delta_2, t) d\delta_1 d\delta_2 = 1$, with n chosen to obtain a periodic continuation of the coefficients.

An exact stationary solution, $\rho_0(\delta_1, \delta_2)$, of (5) may be found when $J=0$. For the finite J case, we can obtain an approximate stationary solution (noting the 2π -periodicity of the phase angles δ_i) via a Fourier expansion of the probability density function, followed by a numerical integration over a finite number (selected to ensure convergence of the expansion) of modes [19]. The expansion converges more rapidly with increasing β and noise intensity $2D$.

Having computed the solution of the FPE (5), we may compute various averaged quantities of interest, e.g. the $\langle I_s \rangle$ vs. Φ_{ex} TC [19]. The TC so obtained, agrees very well with (far costlier) simulations of the dynamical equations (1) with noise, as well as with experimental results [9]. In fact, we may (for $J \neq 0$) perform an inverse β expansion of the probability density function [19], and compute the zeroth-order term analytically. The expansion converges rapidly with increasing β , with even the zeroth-order terms providing very good results for $\beta > 1$.

Using the solution of the FPE (5), we may now compute the average frequency $\langle \dot{\delta}_i \rangle = \langle v_i \rangle$ of each junction:

$$\langle v_i \rangle = \int_0^{2\pi} \int_0^{2\pi} d\delta_1 d\delta_2 v_i(\delta_1, \delta_2) \rho_0(\delta_1, \delta_2). \quad (7)$$

In Fig. 2, we show the average frequency $\langle \dot{\delta}_i \rangle$ as a function of J for the noisy ($D=0.1$) and noiseless case. In the absence of noise, there exists a sharp transition, which corresponds to the bifurcation point that separates the superconducting and running regimes. In the noisy case on the other hand, thermal fluctuations lead to a non-zero average frequency for arbitrary small bias currents J ; the bifurcation is no longer sharp. On the same figure, we show data points obtained via the (deterministic) normal form

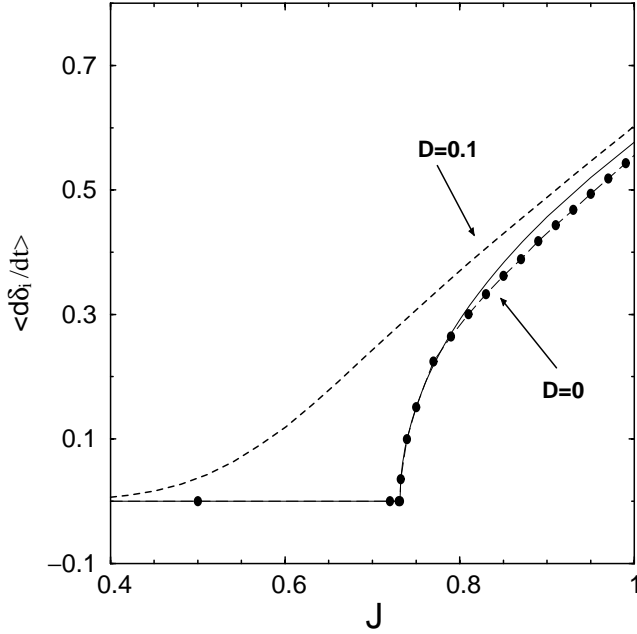


Fig. 2. Running frequency computed via (7) for $D = 0, 0.1$. Data points correspond to $D = 0$ normal form result [5]. $\beta = 5$, $\Phi_{ex} = 0.4$, and D is in dimensional units (time t has been rescaled by τ/I_0 [19]).

calculation [15]; as expected, the agreement with the computed frequency is very good, close to the critical point.

4. Adding an external locking signal

We now augment our normal form with an external time-sinusoidal signal $\varepsilon \sin \omega t$ with ω taken to be close to the running frequency $\omega_0 = T^{-1}$. Then, as ε is increased, the running frequency is pulled towards the injection frequency until the frequencies lock [17]. At this point, one observes a significant lowering of the noise-floor even far away from the injection frequency (Fig. 3). This effect appears to have been first observed in charge density wave experiments [20] and later explained via a simple iterative map model [21]. The above effect provides a cogent explanation for the experimental results shown in Fig. 1. Clearly, in the running regime, the deterministic control parameters (J, Φ_{ex}) can be adjusted to change the spontaneous oscillation frequency. When the running frequency achieves the value of the target frequency, one obtains a sharp resonance. This is evident in Fig. 3 (right), wherein the peak in $\langle I_s \rangle$ occurs precisely at $\omega = 2\pi T^{-1}$. For a small detuning off-resonance mixing sidebands occur in the output PSD, at the expense of energy at the main (i.e., on-resonance) peak; this feature may be exploitable for signal detection [17]. Note that in the SR regime (below the critical point) one does not see a resonance, in keeping with what is already well known [1–3].

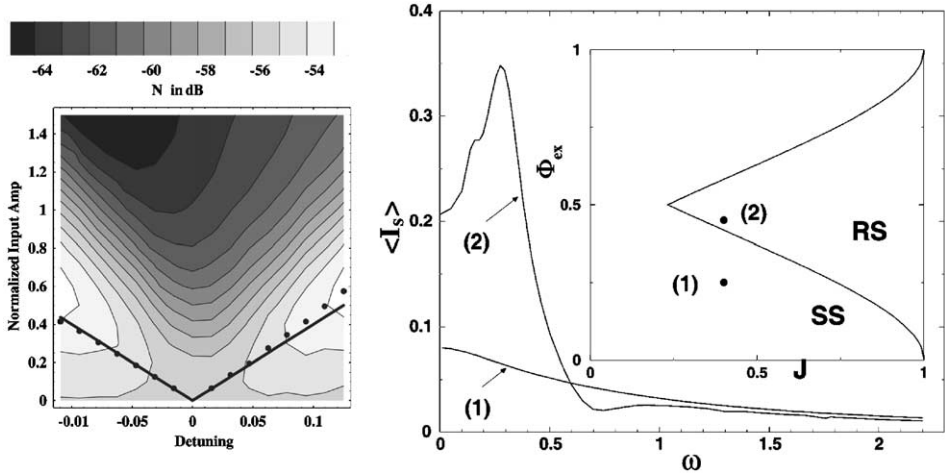


Fig. 3. Left: Low-frequency (3.125% of the running frequency) noise power as a function of input amplitude and detuning. An injection signal amplitude of $q = A_c = 0.002$ just reaches the bifurcation point; “normalized input amplitude” q_N is measured relative to this value. The detuning Δ equals the injection signal frequency ω minus the running state frequency of 0.0479225 rad/s, measured relative to the running frequency. The bold line marks the theoretically predicted minimum amplitude required for locking in the absence of noise, while the dots mark the same quantity as measured via numerical simulation (again, in the absence of noise). $\beta = 2$, $\Phi_{ex} = 0.495$. Right: Deterministic resonance obtained when injection signal frequency matches running frequency in the spontaneously oscillating (RS) regime, with low noise-floor; this contrasts with the static (SS) regime wherein stochastic resonance can occur. The RS and SS regimes are indicated on the accompanying phase diagram that defines the static and oscillating regimes.

Clearly, injection locking to the internal (running) frequency affords the possibility of making the system dynamically “quiet”, and the noise reduction at low frequencies can be particularly useful in sensitive devices like the HTc SQUID. Recent experimental work (Fig. 4) on a dc SQUID demonstrates the noise-floor reduction very well; in experiments, the injection signal may be applied as an addition to the dc bias flux Φ_{ex} , or the bias current I_b with similar effects. Coupling near-identical SQUIDs also has the same effect as applying the locking signal; adjusting the coupling effectively adjusts the running frequencies until perfect locking is achieved for a critical coupling strength [18]; leading to a resonance of the type shown in Fig. 3.

5. Discussion

We have presented an overview of a noise-mediated signal amplification that has the flavor of SR but is actually controllable, in the small noise regime, by adjusting deterministic control parameters that are independent of the input SNR. The spontaneous oscillation frequency in the running regime can be computed, and adjusted via these internal parameters, so that when it matches the applied signal frequency, a resonance (characterized by a lowering of the noise-floor) effect results. For very small noise, the

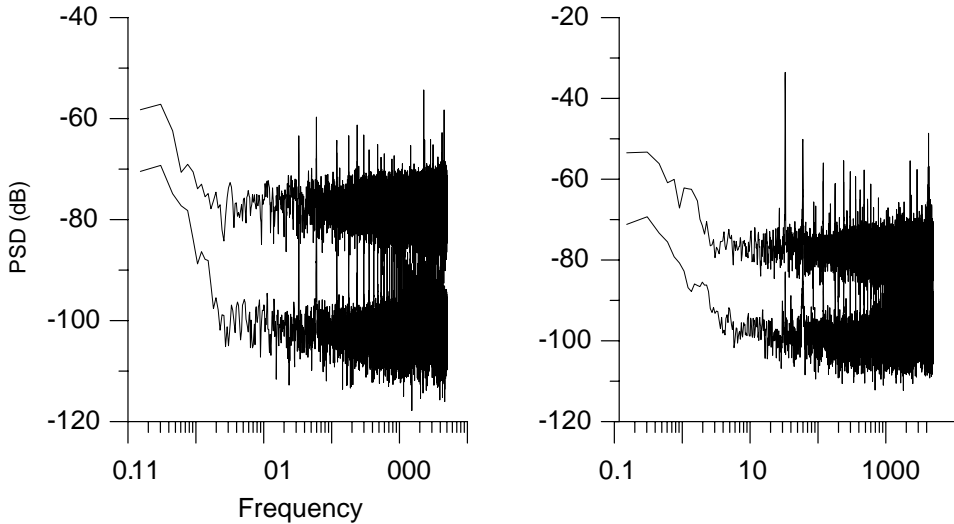


Fig. 4. Measured output power spectral density (PSD) of circulating current) in dc SQUID subject to 970 MHz locking signal applied as a flux bias (left) and current bias (right). Top PSDs in both cases show response PSD without locking signal. In both cases, a low-amplitude sinusoidal (33 Hz) target signal (applied as a flux) is present.

running frequency is near-deterministic, however with increasing noise, the running frequency is dependent on the noise-floor; this manifests itself in a passage time (through the “bottleneck” just into the running regime) distribution that has a noise-dependent mean and mode. Clearly, the noise intensity and the distance $J - J_c$ (for fixed Φ_{ex}) determine whether the mean oscillation frequency is strongly noise-dependent (which was the case in the experiments leading to Fig. 4) or not. The resonance effect can still be realized by locking the external frequency (which could also arise via coupling to another SQUID) to this (now noise-dependent) mean running frequency, thereby moving closer to the “bona fide” description of SR [6].

References

- [1] K. Wiesenfeld, F. Moss, *Nature* 373 (1995) 33.
- [2] A. Bulsara, L. Gammaitoni, *Phys. Today* 49 (1996) 39.
- [3] L. Gammaitoni, P. Hänggi, P. Jung, F. Marchesoni, *Rev. Mod. Phys.* 70 (1998) 223.
- [4] P. Jung, P. Hänggi, *Phys. Rev. A* 44 (1991) 8032.
- [5] R. Fox, Y. Lu, *Phys. Rev. E* 48 (1993) 3390.
- [6] L. Gammaitoni, F. Marchesoni, S. Santucci, *Phys. Rev. Lett.* 74 (1995) 1052.
- [7] A. Hibbs, A. Singaas, A. Bulsara, E. Jacobs, J. Bekkedahl, F. Moss, *J. Appl. Phys.* 77 (1995) 2582.
- [8] R. Rouse, S. Han, J. Lukens, *Appl. Phys. Lett.* 66 (1995) 108.
- [9] A. Hibbs, B. Whitecotton, in: J. Kadtko, A. Bulsara (Eds.), *Applied Nonlinear Dynamics and Stochastic Systems Near the Millenium*, AIP, New York, 1997.
- [10] A. Hibbs, B. Whitecotton, *Appl. Supercond.* 6 (1999) 495.
- [11] A. Barone, G. Paterno, *Physics and Applications of the Josephson Effect*, Wiley, New York, 1982.

- [12] C. Tesche, J. Low. Temp. Phys. 44 (1981) 119.
- [13] M. Inchiosa, A. Bulsara, K. Wiesenfeld, L. Gammaitoni, Phys. Lett. A 252 (1999) 20.
- [14] M. Inchiosa, A. Bulsara, in: D. Broomhead, E. Luchinskaya, P. McClintock, T. Mullin (Eds.), *Stochastic and Chaotic Dynamics at the Lakes*, AIP, New York, 2000.
- [15] K. Wiesenfeld, M. Inchiosa, A. Bulsara, Phys. Rev. B 62 (2000) R9232.
- [16] S. Strogatz, *Nonlinear Dynamics and Chaos*, Perseus Press, New York, 1994.
- [17] M. Inchiosa, V. In, A. Bulsara, K. Wiesenfeld, T. Heath, M. Choi, Phys. Rev. E 63 (2001) 066114.
- [18] J.A. Acebrón, W-J. Rappel, A. Bulsara, Phys. Rev. E 67 (2003) 016210.
- [19] J.A. Acebrón, A. Bulsara, M. Inchiosa, W-J. Rappel, Europhys. Lett. 56 (2001) 354.
- [20] M. Sherwin, A. Zettl, Phys. Rev. B 32 (1985) 5536.
- [21] K. Wiesenfeld, I. Satija, Phys. Rev. B 36 (1987) 2483.